

Skyrmion Echo in a system of interacting Skyrmions

X.-G. Wang¹, Guang-hua Guo¹, A. Dyrdał², J. Barnaś², V. K.

Dugaev³, S. S. P. Parkin⁴, A. Ernst^{4,5} and L. Chotorlishvili³

¹ School of Physics and Electronics, Central South University, Changsha 410083, China

² Faculty of Physics, Adam Mickiewicz University,

ul. Uniwersytetu Poznańskiego 2, 61-614 Poznań, Poland

³ Department of Physics and Medical Engineering,

Rzeszów University of Technology, 35-959 Rzeszów, Poland

⁴ Max Planck Institute of Microstructure Physics, Weinberg 2, D-06120 Halle, Germany

⁵ Institute for Theoretical Physics, Johannes Kepler University, Altenberger Straße 69, 4040 Linz, Austria

(Dated: September 14, 2022)

We consider helical rotation of skyrmions confined in the potentials formed by nano-disks. Based on numerical and analytical calculations we propose the skyrmion echo phenomenon. The physical mechanism of the skyrmion echo formation is also proposed. Due to the distortion of the lattice, impurities, or pinning effect, confined skyrmions experience slightly different local fields, which leads to dephasing of the initial signal. The interaction between skyrmions also can contribute to the dephasing process. However, switching the magnetization direction in the nanodisks (e.g. by spin transfer torque) also switches the helical rotation of the skyrmions from clockwise to anticlockwise (or vice-versa), and this restores the initial signal (which is the essence of skyrmion echo).

Introduction In 1950 Erwin Hahn discovered the effect that is now known as the spin echo [1]. Due to the inhomogeneity of a local magnetic field in solids, nuclear (or electron) spins precess with slightly different frequencies. Therefore, an initially excited pulse decays after a specific time. However, the application of a properly designed pulse reverses the precession direction from clockwise to anticlockwise (or vice-versa), and this restores the initial signal. The dephasing/rephasing mechanism of precessing spins was subsequently explained by Bloom [2]. In this letter, we show that the echo mechanism is applicable not only to precessing spins but also to more complex objects, such as, for instance, skyrmions. Skyrmions are topological solitons discovered in non-Abelian gauge field theories [3–6], and subsequently in condensed matter physics [7, 8]. They have localized robust shapes and additionally possess a topological charge – the conserved quantity underlying their topological protection. Magnetic films without inversion symmetry can host skyrmions and specific skyrmionic magnetic textures described by the local magnetization $\mathbf{M}(\mathbf{r})$ have been studied theoretically and then have been discovered experimentally. Owing to their topological properties and potential applications, skyrmions are currently of great interest, both theoretical and experimental. Skyrmions can exist as independent objects, but can also form regular skyrmion lattices (i.e. skyrmion crystals). For fundamental aspects of skyrmions, we refer to classical handbooks [9, 10]. Concerning modern mathematical aspects of skyrmions we refer to [11]. The key source of the skyrmion formation and non-collinear magnetic textures is either the interfacial Dzyaloshinskii–Moriya interaction (DMI) [12–20], competition between ferromagnetic and antiferromagnetic exchange interactions [21], or bulk DMI in case of antiferromagnetic skyrmions [22, 23]. Individual skyrmions can be pinned by specific confinement potentials, e.g., those created by inhomogeneous

magnetic/electric field [24, 25], defects [26], spin transfer torque [27], or magnetic nanodisks [28, 29]. Recent interest in skyrmionics is focused especially on potential applications of skyrmions in data storage and processing technologies [30–35]. In this letter, we explore the formation of the skyrmion echo in a system of interacting skyrmions. In Fig. 1(a) we present the model considered in this paper. The bottom magnetic thin film hosts several skyrmions. On top of this film there are magnetic nanodisks that confine skyrmions in the regions below these nanodisks. Being confined the skyrmions may perform circular clockwise or anticlockwise motion in these regions, and the winding direction depends on the confined field from the nanodisks. By reversing this field one can switch the direction of the skyrmion winding trajectories, and this behavior can play a role similar to that of the second (rephasing) pulse in the Hahn’s spin echo case. Thus, due to dephasing induced by inhomogeneities in the confining magnetic field, one may observe the skyrmion echo – a phenomenon similar to the spin echo. The inhomogeneous field experienced by skyrmions may be formed in various ways, e.g., from lattice distortions or pinning sites. Skyrmion-skyrmion interactions can also contribute to the dephasing process. Material parameters influence the shape and width of the resonance spectra. Consequently, from the skyrmion echo one can extract information on the host material and on the skyrmion-skyrmion interactions. To describe the process, we exploit the Landau-Lifshitz-Gilbert (LLG) equation:

$$\frac{\partial \mathbf{M}}{\partial t} = -\gamma \mathbf{M} \times \mathbf{H}_{\text{eff}} + \frac{\alpha}{M_s} \mathbf{M} \times \frac{\partial \mathbf{M}}{\partial t}. \quad (1)$$

Here, $\mathbf{M} = M_s \mathbf{m}$, with M_s and \mathbf{m} being the saturation magnetization and unit vector along the magnetization \mathbf{M} , while α is the phenomenological Gilbert damping constant. The total effective magnetic field, \mathbf{H}_{eff} , reads:

$\mathbf{H}_{\text{eff}} = \frac{2A_{\text{ex}}}{\mu_0 M_s} \nabla^2 \mathbf{m} + H_z \mathbf{z} + H_b \mathbf{z} - \frac{1}{\mu_0 M_s} \frac{\delta E_D}{\delta \mathbf{m}}$, where the first term describes the internal exchange field with the exchange stiffness A_{ex} , the second term corresponds to the external magnetic field H_z (\mathbf{z} is a unit vector along the axis z normal to the film), the third term specifies coupling between the thin film and nanodisks, while the last term is the DM field, with the DM interaction energy density $E_D = D_m [(m_z \frac{dm_x}{dx} - m_x \frac{dm_z}{dx}) + (m_z \frac{dm_y}{dy} - m_y \frac{dm_z}{dy})]$ and D_m being the strength of the DM interaction. The field H_b is due to all nanodisks and is nonuniform as contributions from different nanodisks may be different in magnitude. We assume that an individual (say i -th) nanodisk creates the confined field acting only on a single skyrmion, $H_b = H_b^i$. The index i will be omitted in general, and will be included only where necessary. In the supplementary information [36] we show that the main conclusions concerning the skyrmion echo are still valid when the anisotropy and demagnetization fields are included into consideration. In numerical calculations we adopt typical parameters that correspond to Co/heavy-metal multi-layers: $A_{\text{ex}} = 10\text{pJ/m}$, $D_m = 0.2\text{mJ/m}^2$, and $M_s = 1.2 \times 10^6\text{A/m}$. The bias magnetic field $H_z = 100\text{ mT}$ is used for stabilization of the skyrmion structure. The skyrmion width is 45 nm (see supplementary information [36]). The size of the ferromagnetic layer is $3000 \times 240 \times 3\text{nm}^3$. The ferromagnetic layer is discretized with the cells of size $3 \times 3 \times 3\text{nm}^3$. The radius of the upper nanodisks is 12 nm. These nanodisks exert a coupling field $H_b \mathbf{z}$ on the skyrmions in the bottom thin ferromagnetic film. The distance between neighboring nanodisks is 270 nm.

Results: Let us consider now the dynamics of a skyrmion located in the region below a specific nanodisk. This dynamics is described by the position of the skyrmion center (q_x, q_y) with respect to the position of the corresponding nanodisk, at $(0, 0)$. Assume the skyrmion was initially slightly displaced from the center of the nanodisk. When the field exerted by the nanodisk on the skyrmion is negative, $H_b < 0$, the skyrmion moves then along the helix trajectory winding clockwise about the nanodisk center, see Fig. 1(b). The corresponding precession frequency is approximately equal to 0.068 GHz. Upon reversing direction of the field H_b to $H_b > 0$, the skyrmion starts to move gradually away from the nanodisk center with the anticlockwise precession. Interestingly, the frequency of an anticlockwise precession (0.071 GHz) is slightly larger than that of the clockwise one (0.068 GHz). This asymmetry in precession under the opposite magnetic fields H_b and $-H_b$ is confirmed by detailed calculations for different amplitudes of H_b , see Fig. 1(c).

An interesting question is how fast the system responds to the switching between clockwise and anticlockwise regimes. To explore this problem, we quench the sign of the exerted field H_b from -15 mT to 15 mT . Such a quench can be achieved for instance by reversing the magnetization orientation in the nanodisk, e.g., via a strong spin-transfer torque. We find that the skyrmion reacts

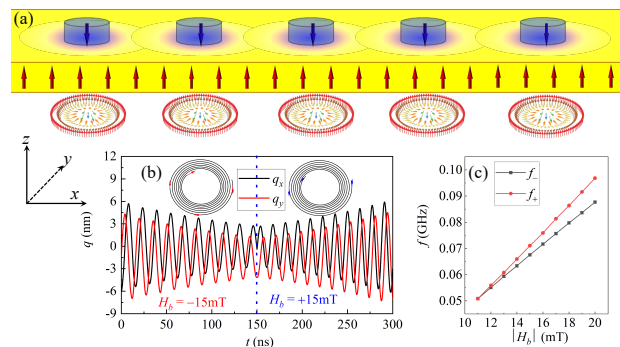


FIG. 1. (a) Schematic of a chain of pinned skyrmions. Skyrmions are created in a thin magnetic film, on top of which there are magnetic nanodisks. The blue arrows show the direction of the field exerted on the skyrmions by the nanodisks. The skyrmions are confined in the regions below the nanodisks. Initially a particular skyrmion is embedded in the vicinity of the center of the corresponding nanodisk. (b) The skyrmion dynamics is described in terms of the position of the skyrmion center (q_x, q_y) with respect to the center of the corresponding nanodisk. For a negative field $H_b = -15\text{ mT}$, the skyrmion moves along the helix trajectory towards the center of the nanodisk $(0, 0)$. Upon the sudden quenching of the field H_b from -15 mT to 15 mT , at $t = 150\text{ ns}$, the skyrmion moves along the helix trajectory away from the center of the nanodisk. (c) Frequencies of the clockwise (f_- , $H_b < 0$) and anticlockwise (f_+ , $H_b > 0$) precessions as a function of the amplitude of the field exerted on the skyrmion by the nanodisk, $|H_b|$. The anticlockwise precession frequency is larger than that of the clockwise one.

almost instantaneously as follows from Fig. 1(b).

We elaborate the experimentally feasible scheme for a skyrmion echo. For the spin echo, the spins initially aligned parallel to the z axis are rotated by a $\pi/2$ pulse applied at $t = 0$, and then they start to precess in the (xy) plane with different Larmor frequencies. The mismatch between these frequencies leads to a dephasing of the precessions of different spins. The second π pulse applied at $t = \tau_0$ reverses the precession direction and rephases the signal. In particular, the refocusing of the spin orientations occurs at $t = 2\tau_0$. Inspired by the idea of the spin echo, we generate a system of $n = 10$ separated skyrmions, that are pinned under the ten nanodisks, see Fig. 1. The coupling fields from these nanodisks are slightly different, inducing different precession frequencies of the ten skyrmions. This can be achieved by a slight variation of the spacer thickness between the nanodisks and magnetic film, as the coupling strength is a function of the spacer thickness [37]. In the model above, the pinning field induced by nanodisk is uniformly distributed and its amplitude varies from 10 mT to 20 mT. Variation of the spacer thickness in the range of 1 nm is sufficient to generate such a change in the pinning field [37, 38]. All skyrmions are initially steered away from the centers of nanodisks in the $-x$ direction. This can be achieved by applying a spin-transfer torque or

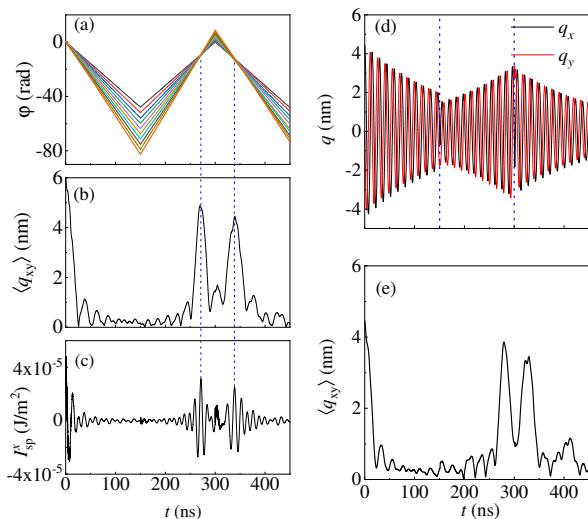


FIG. 2. (a) Evolution of the precession phases $\varphi_i = \arctan(q_y^i/q_x^i)$ for 10 skyrmions. After the time interval 150 ns, the direction of magnetic field H_b in all nanodisks is reversed periodically. (b) The time dependence of the amplitude of skyrmion echo, $\langle q_{xy} \rangle = \frac{1}{n} [(\sum_{i=1}^n q_x^i)^2 + (\sum_{i=1}^n q_y^i)^2]^{1/2}$ (here the average is over all $n = 10$) skyrmions. Blue dashed lines mark the position of the skyrmion echo. (c) The time dependence of the x component of the spin-pumping current I_{sp}^x into an additional heavy metal layer adjacent to the magnetic layer. (d-e) Skyrmion echo induced by current pulse. Dynamics of the upper nanodisks is included *via* the spin transfer torque due to a current pulse in an additional magnetic layer adjacent on top of the layer of nanodisks (saturation magnetization $M_s = 1.4 \times 10^6$ A/m, exchange constant $A_{ex} = 30$ pJ/m, and uniaxial anisotropy along z with constant $K_z = 1 \times 10^6$ J/m³). After a time interval = 150 ns, we periodically reverse the magnetization direction of the nanodisks *via* a strong spin transfer torque, and plot (d) the evolution of x and y coordinates q_x and q_y of the skyrmion position (single skyrmion is plotted while the induced reversal in skyrmion precession applies to all 10 skyrmions), and (e) the averaged amplitude $\langle q_{xy} \rangle$ of all 10 skyrmions.

a nonuniform magnetic field (for details see the supplementary information [36]). At the initial moment, $t = 0$, we simultaneously release all the skyrmions. Different coupling fields lead to dephasing of the skyrmion oscillations, as demonstrated in Fig. 2(a). At $t = 150$ ns, we abruptly reverse the magnetization orientation in all the nanodisks. The skyrmion precessions are then simultaneously reversed, and re-phasing of the signal is achieved at $t = 270$ ns (this is the skyrmion echo). The skyrmion echo signal can be seen clearly in Fig. 2(b), where the average position of the skyrmions along the x -axis is shown. It is evident that the skyrmion echo signal occurs before $2\tau_0 = 300$ ns. The reason for this is the asymmetry between the clockwise and anticlockwise precession frequencies, see Fig. 1(c). After the decay of the skyrmion echo signal, we reverse once again the field H_b for all the skyrmions at $t = 300$ ns. The second sig-

nal of the skyrmion echo now occurs after a shorter time, i.e. at $t = 340$ ns, see Fig. 2(a,b). Apart from the clockwise-anticlockwise precession asymmetry, the trajectory of the skyrmion is not circular but spiral. Since the initial phases are set to zero and the initial positions of the skyrmions are along the $-x$ direction ($\{-q_{max}\}, 0$), the first echo corresponds to the precession phases about $-\pi$, and all skyrmions situated along the $+x$ direction ($\{q_{max}\}, 0$). In turn, the second echo is characterized by the precession phases of -1.9π , and all skyrmions set at $(\{-q_{max}\} \cos(0.1\pi), \{q_{max}\} \sin(0.1\pi))$. The asymmetry in the dephasing and rephasing frequencies leads to a deviation from a perfect echo, i.e., the phase differences between 10 skyrmions are not precisely equal to zero. The skyrmion echo signal occurs at the minimum phase differences for the bias field $H_z = 180$ mT (see the supplementary information [36]).

The skyrmion echo can be detected experimentally by attaching a heavy metal layer (for example a thin Pt layer) below the magnetic layer and exploiting the spin pumping and inverse spin Hall effects. The coherent precession of skyrmions pumps a spin current along the z axis towards the attached metallic layer, $\mathbf{I}_{sp} = \frac{\hbar g_r}{4\pi} (\mathbf{m} \times \frac{\partial \mathbf{m}}{\partial t})$. The relevant spin mixing conductance is assumed to be $g_r = 7 \times 10^{18} \text{m}^{-2}$. By means of the inverse spin Hall effect, the spin pumping current is converted into an electric current (voltage) $J_{SH} = -\theta_{SH} \frac{e}{\hbar} (\mathbf{I}_{sp} \times \mathbf{z})$, where θ_{SH} is the spin-Hall angle. The x component of \mathbf{I}_{sp} (that generates the y component of J_{SH}) in the bottom magnetic layer is shown in Fig. 2(c), where one can clearly see the skyrmion echo signal. To prove that the sign of the field H_b exerted on the skyrmions can be reversed in experiment, we analyse the magnetic dynamics of nanodisks due to a spin-transfer torque induced by a current pulse in an additional layer above the nanodisks. This dynamics is described by the LLG equation with the spin-transfer torque term included. Coupling between the additional layer and a particular nanodisk is introduced by the interlayer coupling field $H_c = \frac{J_c}{\mu_0 M_s t} \mathbf{m}$, and a different coupling strength J_c is assumed for each of the nanodisks. Here t and \mathbf{m} stand for the layer thickness and unit vector along the nanodisk magnetization, respectively. The corresponding numerical results are shown in Fig. 2(d-e). The magnetization of the nanodisks is reversed through the transfer torque applied to the nanodisks from the adjacent layer, $\boldsymbol{\tau} = O_j \mathbf{m} \times \mathbf{p} \times \mathbf{m}$, where $\mathbf{p} = \mathbf{z}$ is the spin polarization orientation of the electrons. The spin transfer torque strength $O_j = \frac{\gamma P \hbar J_e}{2\mu_0 e t M_s}$ is determined by the electric current J_e , thickness $t = 2$ nm, and current polarization degree $P = 0.5$. We applied an ultrashort pulse of amplitude $J_e = 1.7 \times 10^7$ A/cm² and duration of 2 ns. Numerical results plotted in Fig. 2(d-e) show the skyrmion echo signal, and, thus, indirectly also confirm the switching of the magnetization in the nanodisks.

The skyrmion echo can also be described by Thiele's

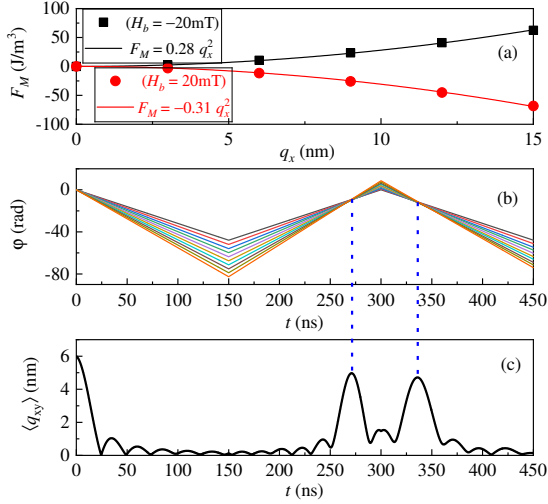


FIG. 3. (a) Averaged (over skyrmion area) magnetic free energy density F_M of the skyrmion as a function of the skyrmion position q_x with respect to the corresponding nanodisk center, $q_y = 0$. The magnetic free energy is extracted from the simulation results, and the data are fitted to the function $F_M = Ar^2$, where $r^2 = q_x^2 + q_y^2$. (b) and (c) Time evolution of the precession phases (b) and amplitude $\langle q_{xy} \rangle = \frac{1}{n} [(\sum_{i=1}^n q_x^i)^2 + (\sum_{i=1}^n q_y^i)^2]^{1/2}$ of 10 skyrmions (c), calculated from the Thiele's equation.

equations [30, 39–41]:

$$\begin{aligned} -\alpha D \partial_t q_x - \partial_t q_y &= -f_x^p - f_x^s, \\ \partial_t q_x - \alpha D \partial_t q_y &= -f_y^p - f_y^s. \end{aligned} \quad (2)$$

Here, $D \approx 1$ stands for the (x,x) and (y,y) components of the dissipative force tensor \mathbf{D} : $\mathbf{D}_{ij} = D$ for $(i, j) = (x, x)$ and $(i, j) = (y, y)$, while $\mathbf{D}_{ij} = 0$ otherwise [39]. In turn, $f_{x,y}^p$ is the force acting on a particular skyrmion due to the corresponding confining potential V , $\mathbf{f}^p = -\nabla V$. $f_{x,y}^p$ and V are determined from F_M , see the supplementary information [36]. We calculate numerically the free energy and fitted it to the analytical result obtained for the quadratic confinement function. The confining potential describes the effect of coupling between the skyrmion and the corresponding nanodisk, and generally may be different for different skyrmions. In particular, we consider $V = cr^2$, where $r^2 = q_x^2 + q_y^2$ and the pinning center is set as $(x, y) = (0, 0)$. Additionally, the neighbouring skyrmions experience a repulsive interaction. As the skyrmions are confined in the areas below the nanodisks, the distance between them can vary only over a small range. Thus, one may assume that the repulsive force in the confinement region is constant. Accordingly, the energy corresponding to the repulsion of two (i -th and j -th) neighbouring skyrmions can then be written as $E_c = -c_u r_d$ (the detailed definition of coupling constant $c_u > 0$ and the distance between skyrmions r_d see in the supplementary information [36]). The repulsion force acting on the i -th skyrmion is

determined as $f_{x,y}^{i,s} = -\partial E_c / \partial q_{x,y}^i$ (and similarly for the j -th skyrmion). Note, the absolute value of the force acting on the skyrmions is equal to c_u and is measured in the units of m/s (because the force in Thiele's equation is normalized to M/γ). In what follows the coefficients c and c_u are phenomenological constants and are tuned to achieve good agreement of the results based on Thiele's equation and on the micromagnetic simulations. To explore the role of the skyrmion-skyrmion interaction we first describe the skyrmion precession in the absence of inter-skyrmion coupling, ($c_u = 0$), and adopt the ansatz $q_x = q_{x0} \exp(i\omega t)$ and $q_y = q_{y0} \exp(i\omega t)$. From the Thiele's equation we derive the equation for the column vector $\mathbf{q} = (q_{x0}, q_{y0})^T$, $\hat{H}\mathbf{q} = \omega\mathbf{q}$. The explicit form of the matrix \hat{H} reads:

$$\hat{H} = \frac{1}{1 + \alpha^2} \begin{pmatrix} -2iac & 2ic \\ -2ic & -2iac \end{pmatrix}. \quad (3)$$

The eigenfrequencies of the matrix \hat{H} read: $\omega_{\pm} = \pm \frac{2c(1 \pm i\alpha)}{1 + \alpha^2}$. The eigenvectors corresponding to the eigenvalues ω_+ and ω_- have the forms $(-i, 1)$ and $(i, 1)$, respectively. The real parts of the eigenfrequencies correspond to the skyrmion precession frequencies, and the imaginary parts describe the attenuation. As one can see in Fig. 3(a), the coefficient of the confinement potential c is positive for a negative field H_b . Therefore, the steady clockwise precession is described by the frequency ω_+ and the corresponding vector $(-i, 1)$. In turn, for positive field, $H_b > 0$, the parameter c is negative with a larger absolute value. The corresponding frequency ω_- has larger real part as well and the vector $(i, 1)$ corresponds to counter-clockwise precession. This has been also confirmed in numerical simulations. To achieve a good agreement with the results of micromagnetic simulations, we adjusted the value of c for different values of H_b , and calculated the time dependence of the precession phase and total oscillations, as plotted in Fig. 3. The analytical results are in good agreement with those obtained from micromagnetic simulations, see Fig. 2. To analyze the influence of coupling between skyrmions, we explored the skyrmion echo as a function of the distance d_s between skyrmions (in the experiment d_s is equal to the distance between nanodisks). The coupling strength between skyrmions increases with decreasing d_s [21]. As shown in Fig. 4, the coupling energy and coupling strength exponentially decay for large d_s , while the echo signal increases and saturates. When decreasing d_s , the coupling strength increases and the echo signal $\langle q_{xy} \rangle$ becomes reduced. The observed effect has a clear physical explanation: For the short d_s , the observed non-monotonic behavior is related to collective oscillations caused by the strong coupling between skyrmions. For $d_s > 150$ nm, the interaction between skyrmions is weak, and the echo signal is insensitive to the distance between skyrmions, see Fig. 4. One can extract information on the skyrmion-skyrmion interaction strength by performing echo experiments for $d_s < 150$ nm.

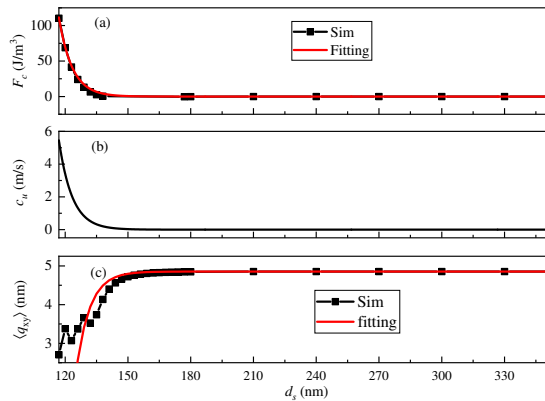


FIG. 4. (a) Dependence of the magnetic free energy density F_c on the distance d_s between neighboring skyrmions. The magnetic free energy is extracted from the simulation results. The energy $F_c(d_s)$ fits to the exponential function $F_c = A_0 \exp(-d_s/\xi)$ with the decaying length $\xi = 6.4$ nm. (b) The coupling strength c_u extracted from linear expansion of the energy profile in the vicinity of the skyrmion center. (c) The amplitude $\langle q_{xy} \rangle$ of the skyrmion echo as a function of the distance d_s between neighboring skyrmions. Amplitudes are fitted to the exponential function $\langle q_{xy} \rangle = I_1 - I_0 \exp(-d_s/\xi)$. The bias field is $H_z = 100$ mT.

Summary and conclusions: The inhomogeneous field leads to a dephasing of an initial signal. Switching the magnetization of the nanodisks (e.g due to the application of a spin-polarized torque) turns the dephasing process into a rephasing one, and after a certain time, the signal of the skyrmion echo is recovered. The proposed skyrmion echo is experimentally feasible and can be detected by exploiting the spin pumping and inverse spin Hall effects. The skyrmion echo will also be important for the coupled systems of skyrmions and superconducting vortices [42], i.e. for a hypothetical superconducting vortex echo.

Acknowledgements: The work is supported by Shota Rustaveli National Science Foundation of Georgia (SRNSFG) (Grant No. FR-19-4049), the National Natural Science Foundation of China (Grants No. 12174452, No. 11704415 and No. 12074437), the Natural Science Foundation of Hunan Province of China (Grants No. 2022JJ20050 and No. 2021JJ30784), and by the National Science Center in Poland by the Norwegian Financial Mechanism 2014-2021 under the Polish-Norwegian Research Project NCN GRIEG (2Dtronics) no. 2019/34/H/ST3/00515 (AD,JB), the FWF International Project I 5384, and as a research Project No. DEC-2017/27/B/ST3/ 02881 (VKD).

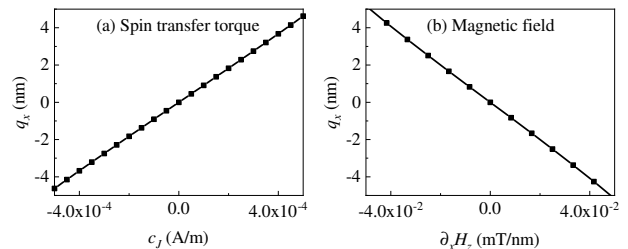


FIG. S1. The initial displacement of a skyrmion, q_x , along the x axis, driven by spin transfer torque (a) or spatially varying external magnetic field (b).

I. SUPPLEMENTARY INFORMATION

A. Numerical simulation details

The LLG equation is numerically solved employing a fifth-order Runge-Kutta scheme with a fixed time step of 0.5 ps. We adopted the finite difference approximation, and discretized the ferromagnetic layer in the unit simulation cells $s \times s \times s$ with $s = 3$ nm. To quantitatively characterize the skyrmion structure, we used the skyrmion topological charge density $c = (1/4\pi) \mathbf{m} \cdot (\partial_x \mathbf{m} \times \partial_y \mathbf{m})$, and the total topological charge $C = \int d^2 \mathbf{r} c$. The position of i -th skyrmion centre, $\mathbf{q}_i = (q_x^i, q_y^i)$, is weighed by the topological charge: $\mathbf{q}_i = \int_1 d^2 \mathbf{r} \mathbf{m} \cdot (\partial_x \mathbf{m} \times \partial_y \mathbf{m}) \mathbf{r} / \int d^2 \mathbf{r} \mathbf{m} \cdot (\partial_x \mathbf{m} \times \partial_y \mathbf{m})$ [43]. For each skyrmion the integration range is limited by the area near the corresponding pinning center. When integrating over the whole magnetic layer one finds $\sum_{i=1}^n \mathbf{q}^i$.

To shift slightly the initial positions of skyrmions one can apply a spin-transfer torque [30] or a magnetic field [44]. For example, the applied spin transfer torque $\boldsymbol{\tau}_{\text{STT}} = \gamma c_j \mathbf{m} \times \mathbf{y} \times \mathbf{m}$, with the electron polarization along the y axis, steers the skyrmion center in the x direction. As shown in Fig. S1(a), positive (negative) c_j shifts the skyrmion along $+(-)x$ direction, and the induced displacement q_x depends linearly on c_j (or electric current density). The same can be achieved by spatially inhomogeneous magnetic field H_z . The gradient of the field, $\partial_x H_z$, linearly shifts the skyrmion along the axis $\pm x$ and the sign depends on the sign of the gradient $\partial_x H_z$, as it is shown in Fig. S1(b).

To exclude numerical artifacts of the coarse-graining procedure, we performed calculations for the smaller size of the cell, $s = 1$ nm. As it is shown in Fig. S2, the obtained result is almost identical with that obtained for $s = 3$ nm. The difference in precession frequencies is about 5%. The radius 45 nm of the skyrmion is larger than the radius of the nanodisk 12 nm. Confinement of the skyrmion by nanodisk is quite efficient.

We have also analyzed the impact of the Gilbert damping constant α and found that the magnitude of damping parameter α has a significant influence on the skyrmion

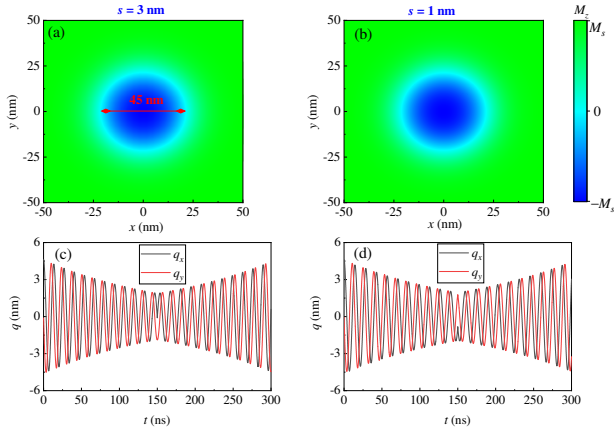


FIG. S2. (a,b) The M_z component of the skyrmion magnetic texture for two different values of cell size: $s = 3$ nm (a) and $s = 1$ nm (b). (c,d) Precession of the single skyrmion around the center $(0, 0)$ of the nanodisk for $s = 3$ nm (c) and $s = 1$ nm (d). At $t = 150$ ns, the direction of the coupling field H_b is changed from -15 mT to 15 mT. The bias magnetic field $H_z = 100$ mT and the size of the stable skyrmion is about 45 nm.

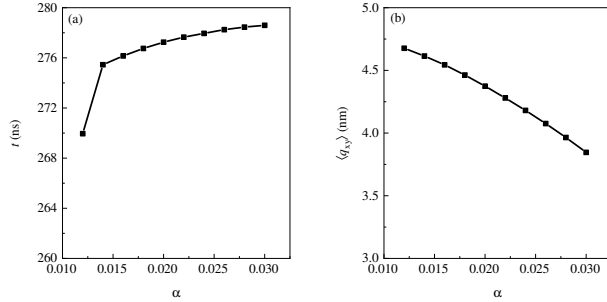


FIG. S3. (a) Dependence of the rephasing time on the damping constant α . For a stronger damping, the rephasing process becomes slower. (b) The amplitude of skyrmion echo $\langle q_{xy} \rangle = \frac{1}{n} [(\sum_{i=1}^n q_x^i)^2 + (\sum_{i=1}^n q_y^i)^2]^{1/2}$ as a function of the damping constant α . The bias field is assumed $H_z = 100$ mT. The direction of the coupling field in all nanodisks is reversed at $t = 150$ ns, and the distance between neighboring skyrmions is $d_s = 270$ nm.

relaxation and on the rephasing of the echo, see Fig. S3. The enhanced damping slows down the rephasing process and also decreases the amplitude of the skyrmion echo.

In the main text, the averaged magnetic energy density is calculated from the formula $F_M = -\frac{\mu_0 M_s}{S} \int \mathbf{m} \cdot \mathbf{H}_{\text{eff}} d^2r$ applied to the region inside of the skyrmion (cross-section S). The spatial profile of the magnetization vector \mathbf{m} and the effective field \mathbf{H}_{eff} are obtained from simulation results. To obtain the position-dependent F_M curve (Fig. 3(a) in the main text), we fixed the initial stable skyrmion texture and gradually moved the pinning center along the x axis. Then, from the spatial gradient of F_M , one

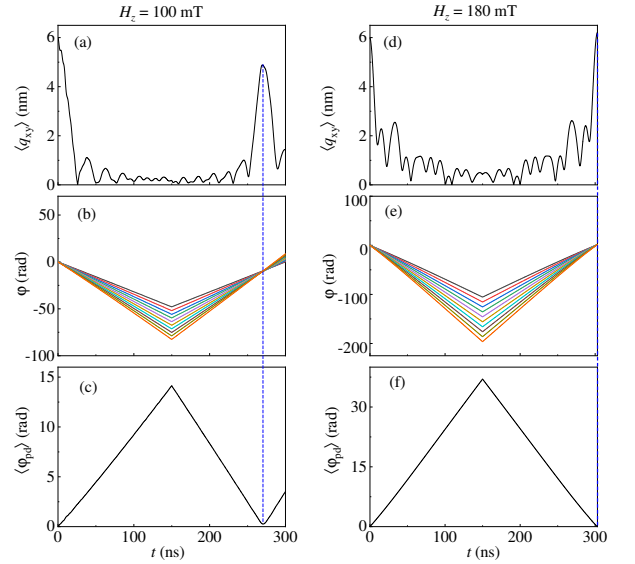


FIG. S4. (a,d) Time dependence of the amplitude of skyrmion echo averaged over all ($n=10$) skyrmions, $\langle q_{xy} \rangle = \frac{1}{n} [(\sum_{i=1}^n q_x^i)^2 + (\sum_{i=1}^n q_y^i)^2]^{1/2}$, plotted for two different bias fields $H_z = 100$ mT and $H_z = 180$ mT. (b,e) Evolution of the precession phases of all $n = 10$ skyrmions. (c,f) The averaged phase differences between the $n = 10$ skyrmions, evaluated as $\langle \varphi_{pd} \rangle = \sum_{i=1}^n \sum_{j=1}^n (\varphi_j - \varphi_i) / n^2$. The direction of the coupling field in all nanodisks is reversed at $t = 150$ ns, and the distance between neighboring skyrmions is $d_s = 270$ nm.

obtains the real phenomenological confining force acting on the skyrmion. However, due to specific normalization of the Thiele equation, to implement the confining force into this equation one needs to normalize accordingly the confining potential. Therefore, we introduce the relevant potential V as $V = c_p F_M = (c_p A) r^2 = c r^2$, and in Fig. 1(c) in the main text) we used $c_p = 0.31 \times 10^{-9} \text{m}^5/\text{Js}$. The confining force $f_{x,y}^p$ is the give by the gradient of V , $f_{x,y}^p = -\partial V / \partial x, y$.

B. Different bias field and distance

The dephasing and rephasing times are slightly different. This fact can have an impact on the signal of the skyrmion echo. Therefore it is necessary to evaluate the quality of rephasing of the skyrmion echo. Let us define average difference between the skyrmion phases through the equation $\langle \varphi_{pd} \rangle = \sum_{i=1}^n \sum_{j=1}^n (\varphi_j - \varphi_i) / n^2$. In the case of exact rephasing one finds $\langle \varphi_{pd} \rangle = 0$. In Fig. S4 we see that signal of the skyrmion echo appears when $\langle \varphi_{pd} \rangle$ is minimal. For the bias field $H_z = 100$ mT, the minimum of phase differences is $\langle \varphi_{pd} \rangle = 0.25$ at $t = 270$ ns. With increasing H_z , the asymmetry between dephasing and rephasing times gradually decreases. At $H_z = 180$ mT, the minimum of $\langle \varphi_{pd} \rangle \approx 0$ for $t = 300$ ns indicates on a perfect rephasing, and the amplitude of the corresponding echo signal becomes larger. With a further

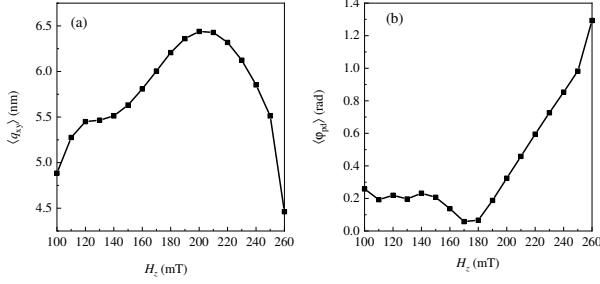


FIG. S5. (a) The amplitude $\langle q_{xy} \rangle$ and (b) minimum phase difference $\langle \varphi_{pd} \rangle$ of the skyrmion echo as a function of the bias field H_z . The distance between neighboring skyrmions is $d_s = 270$ nm.

increase of H_z , the rephasing time becomes larger and the minimum of $\langle \varphi_{pd} \rangle$ increases again, as is shown in Fig. S5. The amplitude of the skyrmion echo, $\langle q_{xy} \rangle$, increases until $H_z = 210$ mT, while $\langle \varphi_{pd} \rangle$ is not zero. The difference between behavior of $\langle q_{xy} \rangle$ and $\langle \varphi_{pd} \rangle$ is related to the bigger rephasing time. The skyrmion trajectory becomes larger in the rephasing stage. For example, at $H_z = 210$ mT, the echo (minimum of $\langle \varphi_{pd} \rangle$) is achieved at $t = 330$ ns, and larger rephasing time leads to the greater amplitude $\langle q_{xy} \rangle$.

Furthermore, as discussed in the main text, the skyrmion-skyrmion coupling strength c_u also affects the skyrmion echo strength. We suggest varying the distance d_s between neighboring skyrmions (and nanodisks) to reproduce the experimentally feasible small dispersion of the coupling strength. According to Ref. [45–48], the coupling strength between skyrmions increases with decreasing distance d_s . In the analysis, the coupling strength c_u is defined from the linear ansatz. First, from the numerical simulation we extracted the magnetic free energy density F_c as a function of the distance d_s (also the distance between two neighboring skyrmions), which fits to the exponential function $F_c = A_0 \exp(-d_s/\xi)$. For application in the Thiele equation, the repulsion energy is given by the formula, $E_c = c_p A_0 \exp(-r_d/\xi)$, where $r_d = \sqrt{(d_s + q_x^i - q_x^j)^2 + (q_y^i - q_y^j)^2}$ is the distance between two skyrmions. From $f_{x,y}^{i,s} = -\partial E_c / \partial q_{x,y}^i$, we find the repulsion forces $f_x^{i,s} = E_c(d_s + q_x^i - q_x^j)/\xi r_d$ and $f_y^{i,s} = E_c(q_y^i - q_y^j)/\xi r_d$. As the skyrmion oscillates around the pinning center with a small amplitude, in this small range we adopted the linear ansatz $E_c = -c_u r_d$. The forces can be then rewritten as $f_x^{i,s} = c_u(d_s + q_x^i - q_x^j)/r_d$ and $f_y^{i,s} = c_u(q_y^i - q_y^j)/r_d$. The coupling strength is determined through comparing two expressions $c_u = E_c/\xi = c_p A_0 \exp(-r_d/\xi)/\xi$.

An interesting question is the change of the echo strength with the pulse duration τ_0 . From the simulation results shown in Fig. S6(a), one can see that the amplitude of the echo decreases with the duration of the pulse τ_0 and slightly fluctuates. We analyze this dependence

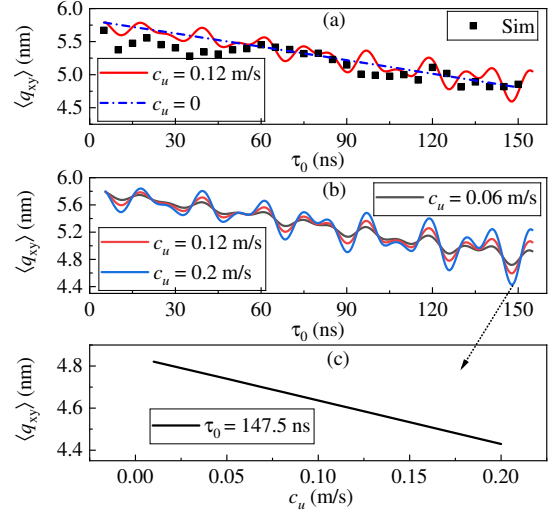


FIG. S6. (a) Amplitude of the skyrmion echo $\langle q_{xy} \rangle = \frac{1}{n} [(\sum_{i=1}^n q_x^i)^2 + (\sum_{i=1}^n q_y^i)^2]^{1/2}$ as a function of pulse duration τ_0 . Black squares correspond to the micromagnetic simulations, whereas the blue dashed line (the coupling strength $c_u = 0$) and the red solid circles (the coupling strength $c_u = 0.12$ m/s) are obtained from Thiele's equation. (b) Numerical solution of Thiele's equation, for different values of c_u . (c) Dependence of the amplitude of skyrmion echo on the strength of inter-skyrmion coupling c_u for $\tau_0 = 147.5$ ns.

by the numerical solution of Thiele's equation. When all skyrmions are independent ($c_u = 0$), the echo strength decreases monotonically with τ_0 (Fig. S6(a)). A strong enough coupling ($c_u = 0.12$ m/s) leads to fluctuations similar to those observed in the micromagnetic simulations. With the increase of the skyrmion-skyrmion interaction c_u , the fluctuation amplitude increases, but the shape of the curve remains unchanged.

We note that opposite to the conventional spin-echo, the trajectories of the skyrmions are helices and therefore for individual skyrmions $\langle q_{xy} \rangle = [(q_x^i)^2 + (q_y^i)^2]^{1/2}$ are not circles of constant radius [45]. This difference should be taken into account in order to understand behavior of the skyrmion echo amplitude with the coupling strength and pulse duration.

C. Influences of demagnetization field

For a more realistic discussion, we analyze the influences of dipole-dipole interaction on the skyrmion echo. In the simulation, we also include the uniaxial anisotropy field $\frac{2K_u}{\mu_0 M_s} m_z \mathbf{z}$ along the z axis with the constant $K_u = 0.905 \times 10^6 \text{ Jm}^{-3}$, as well as the demagnetization field,

$$\mathbf{H}_{\text{demag}}(\mathbf{r}) = -\frac{M_s}{4\pi} \int_V \nabla \nabla' \frac{\mathbf{m}(\mathbf{r}')}{|\mathbf{r} - \mathbf{r}'|} d\mathbf{r}'. \quad (\text{S1})$$

The film is uniformly magnetized along the z axis and the effective field of uniaxial anisotropy $1.2 \times 10^6 \text{ A/m}$ is

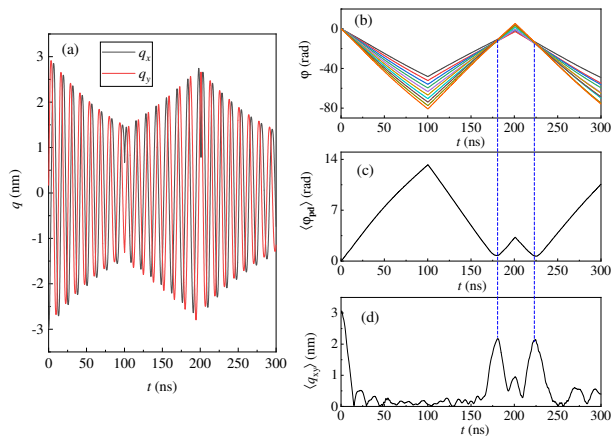


FIG. S7. The effect of the demagnetization field. (a) Dynamics of single skyrmion precession around the center $(0, 0)$ of the nanodisk. (b-d) Time evolution of the precession phases, phase difference $\langle \varphi_{pd} \rangle$, and averaged $\langle q_{xy} \rangle$ over ten skyrmions calculated from micromagnetic simulations. The direction of coupling field H_b in the nanodisk is reversed periodically after 100 ns, and the distance between neighboring skyrmions (and thus nanodisks) is $d_s = 540$ nm.

partially compensated by the static demagnetization field $-N_z M_s$, with the film demagnetization factor $N_z = 1$. We found a slight effect of the dipole-dipole interaction on the skyrmion dynamics. The main conclusions concerning the skyrmion echo still hold. The results for the skyrmion echo in the system with the demagnetization field are shown in Fig. S7. We again studied the same system of $n = 10$ separated skyrmions pinned under ten nanodisks with slightly different coupling fields, and the distance between neighboring nanodisks was $d_s = 540$ nm. One can clearly see the skyrmions dephasing and rephasing, minimum in the phase difference $\langle \varphi_{pd} \rangle$, and the skyrmion echo.

-
- [1] A. Abragam, *The principles of nuclear magnetism*, 32 (Oxford university press, 1961).
- [2] A. L. Bloom, Nuclear induction in inhomogeneous fields, *Phys. Rev.* **98**, 1105 (1955).
- [3] B. J. Schroers, Bogomol'nyi solitons in a gauged o(3) sigma model, *Phys. Lett. B* **356**, 291 (1995).
- [4] A. Samoilenka and Y. Shnir, Gauged baby skyrme model with a chern-simons term, *Phys. Rev. D* **95**, 045002 (2017).
- [5] R. A. Battye and M. Haberichter, Isospinning baby skyrmion solutions, *Phys. Rev. D* **88**, 125016 (2013).
- [6] P. Jennings and T. Winyard, Broken planar skyrmions—statics and dynamics, *J. High Energy Phys.* **2014**, 122 (2014).
- [7] S. Seki, X. Yu, S. Ishiwata, and Y. Tokura, Observation of skyrmions in a multiferroic material, *Science* **336**, 198 (2012).
- [8] M. Wilson, A. Butenko, A. Bogdanov, and T. Monchisky, Chiral skyrmions in cubic helimagnet films: The role of uniaxial anisotropy, *Phys. Rev. B* **89**, 094411 (2014).
- [9] R. Rajaraman, Solitons and instantons. amsterdam, ny, (1982).
- [10] A. Altland and B. D. Simons, *Condensed matter field theory* (Cambridge university press, 2010).
- [11] B. Barton-Singer, C. Ross, and B. J. Schroers, Magnetic skyrmions at critical coupling, *Commun. Math. Phys.* , **1** (2020).
- [12] J. White, K. Prša, P. Huang, A. Omrani, I. Živković, M. Bartkowiak, H. Berger, A. Magrez, J. Gavilano, G. Nagy, *et al.*, Electric-field-induced skyrmion distortion and giant lattice rotation in the magnetoelectric insulator Cu_2OSeO_3 , *Phys. Rev. Lett.* **113**, 107203 (2014).
- [13] A. Derras-Chouk, E. M. Chudnovsky, and D. A. Garanin, Quantum collapse of a magnetic skyrmion, *Phys. Rev. B* **98**, 024423 (2018).
- [14] S. Haldar, S. von Malottki, S. Meyer, P. F. Bessarab, and S. Heinze, First-principles prediction of sub-10-nm skyrmions in pd/fe bilayers on rh(111), *Phys. Rev. B* **98**, 060413 (2018).
- [15] C. Psaroudaki, S. Hoffman, J. Klinovaja, and D. Loss, Quantum dynamics of skyrmions in chiral magnets, *Phys. Rev. X* **7**, 041045 (2017).
- [16] K. A. van Hoogdalem, Y. Tserkovnyak, and D. Loss, Magnetic texture-induced thermal hall effects, *Phys. Rev. B* **87**, 024402 (2013).
- [17] S. Rohart, J. Miltat, and A. Thiaville, Path to collapse for an isolated néel skyrmion, *Phys. Rev. B* **93**, 214412 (2016).
- [18] S. Tsesses, E. Ostrovsky, K. Cohen, B. Gjonaj, N. Lindner, and G. Bartal, Optical skyrmion lattice in evanescent electromagnetic fields, *Science* **361**, 993 (2018).
- [19] X.-g. Wang, L. Chotorlishvili, G.-h. Guo, and J. Berakdar, Electric field controlled spin waveguide phase shifter in yig, *J. Appl. Phys.* **124**, 073903 (2018).
- [20] X.-g. Wang, L. Chotorlishvili, G.-h. Guo, C.-L. Jia, and J. Berakdar, Thermally assisted skyrmion drag in a nonuniform electric field, *Phys. Rev. B* **99**, 064426 (2019).
- [21] A. Leonov and M. Mostovoy, Multiply periodic states and isolated skyrmions in an anisotropic frustrated magnet, *Nat. Commun.* **6**, 1 (2015).
- [22] X. Zhang, Y. Zhou, and M. Ezawa, Antiferromagnetic skyrmion: Stability, creation and manipulation, *Sci. Rep.* **6**, 24795 (2016).
- [23] J. Barker and O. A. Tretiakov, Static and dynamical properties of antiferromagnetic skyrmions in the presence of applied current and temperature, *Phys. Rev. Lett.* **116**, 147203 (2016).

- [24] C. Wang, D. Xiao, X. Chen, Y. Zhou, and Y. Liu, Manipulating and trapping skyrmions by magnetic field gradients, *New J. Phys.* **19**, 083008 (2017).
- [25] X.-G. Wang, L. Chotorlishvili, V. K. Dugaev, A. Ernst, I. V. Maznichenko, N. Arnold, C. Jia, J. Berakdar, I. Mertig, and J. Barnaś, The optical tweezer of skyrmions, *npj Comput. Mater.* **6**, 140 (2020).
- [26] C. Hanneken, A. Kubetzka, K. von Bergmann, and R. Wiesendanger, Pinning and movement of individual nanoscale magnetic skyrmions via defects, *New J. Phys.* **18**, 055009 (2016).
- [27] F. Ma, Y. Zhou, H. B. Braun, and W. S. Lew, Skyrmion-based dynamic magnonic crystal, *Nano Lett.* **15**, 4029 (2015).
- [28] H. Z. Wu, B. F. Miao, L. Sun, D. Wu, and H. F. Ding, Hybrid magnetic skyrmion, *Phys. Rev. B* **95**, 174416 (2017).
- [29] L. Sun, R. X. Cao, B. F. Miao, Z. Feng, B. You, D. Wu, W. Zhang, A. Hu, and H. F. Ding, Creating an artificial two-dimensional skyrmion crystal by nanopatterning, *Phys. Rev. Lett.* **110**, 167201 (2013).
- [30] R. Tomasello, E. Martinez, R. Zivieri, L. Torres, M. Carpentieri, and G. Finocchio, A strategy for the design of skyrmion racetrack memories, *Sci. Rep.* **4**, 6784 (2014).
- [31] S. Luo and L. You, Skyrmion devices for memory and logic applications, *APL Mater.* **9**, 050901 (2021).
- [32] J. Zázvorka, F. Jakobs, D. Heinze, N. Keil, S. Kromin, S. Jaiswal, K. Litzius, G. Jakob, P. Virnau, D. Pinna, K. Everschor-Sitte, L. Rózsa, A. Donges, U. Nowak, and M. Kläui, Thermal skyrmion diffusion used in a reshuffler device, *Nat. Nanotechnol.* **14**, 658 (2019).
- [33] S. Zhang, A. A. Baker, S. Komineas, and T. Hesjedal, Topological computation based on direct magnetic logic communication, *Scientific Reports* **5**, 15773 (2015).
- [34] A. Fert, V. Cros, and J. Sampaio, Skyrmions on the track, *Nature Nanotech.* **8**, 152 (2013).
- [35] R. Wiesendanger, Nanoscale magnetic skyrmions in metallic films and multilayers: a new twist for spintronics, *Nat. Rev. Mater.* **1**, 16044 (2016).
- [36] See Supplemental Material at [URL will be inserted by publisher] for numerical simulation details and influences of different bias field, distance, and demagnetization field, which includes Refs. [43–48].
- [37] P. Bruno, Theory of interlayer exchange interactions in magnetic multilayers, *Journal of Physics: Condensed Matter* **11**, 9403 (1999).
- [38] P. J. H. Bloemen, M. T. Johnson, M. T. H. van de Vorst, R. Coehoorn, J. J. de Vries, R. Jungblut, J. aan de Stegge, A. Reinders, and W. J. M. de Jonge, Magnetic layer thickness dependence of the interlayer exchange coupling in (001) co/cu/co, *Phys. Rev. Lett.* **72**, 764 (1994).
- [39] J. Seidel, *Topological Structures in Ferromagnetic Materials. Domain Walls, Vortices and Skyrmions*, Springer Series in Materials Science (Springer International Publishing, 2016).
- [40] J. Iwasaki, M. Mochizuki, and N. Nagaosa, Universal current-velocity relation of skyrmion motion in chiral magnets, *Nat. Commun.* **4**, 1463 (2013).
- [41] A. A. Kovalev, Skyrmionic spin seebeck effect via dissipative thermomagnonic torques, *Phys. Rev. B* **89**, 241101 (2014).
- [42] S. M. Dahir, A. F. Volkov, and I. M. Eremin, Interaction of skyrmions and pearl vortices in superconductor-chiral ferromagnet heterostructures, *Phys. Rev. Lett.* **122**, 097001 (2019).
- [43] L. Kong and J. Zang, Dynamics of an insulating skyrmion under a temperature gradient, *Phys. Rev. Lett.* **111**, 067203 (2013).
- [44] S. Komineas and N. Papanicolaou, Skyrmion dynamics in chiral ferromagnets, *Phys. Rev. B* **92**, 064412 (2015).
- [45] X.-G. Wang, L. Chotorlishvili, N. Arnold, V. K. Dugaev, I. Maznichenko, J. Barnaś, P. A. Buczek, S. S. P. Parkin, and A. Ernst, Plasmonic skyrmion lattice based on the magnetoelectric effect, *Phys. Rev. Lett.* **125**, 227201 (2020).
- [46] A. O. Leonov and M. Mostovoy, Multiply periodic states and isolated skyrmions in an anisotropic frustrated magnet, *Nat. Commun.* **6**, 8275 (2015).
- [47] S.-Z. Lin, C. Reichhardt, C. D. Batista, and A. Saxena, Particle model for skyrmions in metallic chiral magnets: Dynamics, pinning, and creep, *Phys. Rev. B* **87**, 214419 (2013).
- [48] Y. A. Kharkov, O. P. Sushkov, and M. Mostovoy, Bound states of skyrmions and merons near the lifshitz point, *Phys. Rev. Lett.* **119**, 207201 (2017).